ELM Dynamic Simulation for Detached Divertor Plasmas Using One-Dimensional Fluid Code*)

Yue LI, Satoshi TOGO[1)], Tomonori TAKIZUKA[2)] and Yuichi OGAWA

Graduate School of Frontier Sciences, The University of Tokyo, Kashiwa 277-8568, Japan
[1)]*Plasma Research Center, University of Tsukuba, Tsukuba 305-8577, Japan*
[2)]*Graduate School of Engineering, Osaka University, Suita 565-0871, Japan*

(Received 27 December 2017 / Accepted 2 April 2018)

We investigate the dynamic response of plasma detachment against the Edge Localized Mode (ELM) using a one-dimensional fluid code. It is found that the heat flux to the target plate after an ELM crash in the detachment starts to increase with a delay, contrary to the sudden increase in the attachment. Larger electron heat flux and smaller ion heat flux to the plate are found in the detachment due to the strong equipartition between electron and ion temperatures, while their heat fluxes are similar in the attachment. In addition, we find the reverse flow in the detachment caused by ELM unbalancing the plasma pressure. Finally, we examine the grassy-ELMs, and find the accumulation of the heat flux pulses in the detached divertor.

Keywords: ELM, detached plasma, one-dimensional fluid code, dynamic response, reverse flow

DOI: 10.1585/pfr.13.3403054

1. Introduction

For designing the divertor of a next-generation fusion reactor, the most promising method to reduce the divertor heat load is the plasma detachment. However, the Edge Localized Mode (ELM) in an H-mode tokamak plasma can affect the plasma detachment [1, 2]. Therefore, it is important to confirm whether the plasma detachment is still an efficient method or not to control the transiently enhanced heat and particle loads due to ELM.

We have been developing a one-dimensional (1D) scrape off layer - divertor (SOL-DIV) fluid code for studying detachment plasma [3]. In this research, we attempt to investigate ELM dynamic behaviors in the plasma detachment using a simple 1D code, although the physics of plasma detachment has still not fully been understood and the current divertor simulation codes are applied basically to study static behaviors of plasma detachment. Considering the fact that the characteristics of ELM energy and particle losses have been investigated much in ASDEX Upgrade [4], we use the parameters in Refs. [4–6] for the present research as shown in Table 1.

In this paper, we study ELM dynamic behaviors in the plasma detachment through adjusting amplitudes of ELM to type I ELM and grassy ELMs. In the case of type I ELM, we focus on the effect of fraction of impurity density on the reverse flow which is observed near the target plate. On the other hand, in the case of grassy ELMs, we focus on the radiation effect which makes the difference of ELM heat fluxes between attachment and detachment much larger than that in the case of type I ELM.

Table 1 Basic parameters based on ASDEX Upgrade plasma.

Pitch angle θ	6 °
Parallel system length L	44.0 m
Parallel SOL length L_{SOL}	35.2 m
Parallel DIV length L_{DIV}	4.4 m
SOL width d_{SOL}	2.0 cm
Separatrix surface area A_{sep}	40.0 m^2
Carbon impurity fraction r_{imp}	1.0 %

2. Simulation Model

The geometry of this model is shown as Fig. 1. Two divertor plates are located at $s = 0$ and $s = L$, where s represents the coordinate in the parallel direction to the magnetic field lines in a tokamak SOL-DIV plasmas. L_{core} and L_{ELM} denote the ranges of steady-state core source and pulsed ELM source, respectively. In the present calculation, for simplicity, both sources are given symmetrically in space with $L_{\mathrm{core}} = L_{\mathrm{SOL}}$ and $L_{\mathrm{ELM}} = L_{\mathrm{SOL}}/2$.

We have been developing a 1D plasma fluid model based on the Braginskii equations [7] as shown in Eqs. (1 - 4) for density n, parallel flow velocity V, ion temperature T_{i} and electron temperature T_{e}. Source terms are denoted by S, M_{m} and $Q_{\mathrm{i/e}}$, respectively.

$$\frac{\partial n}{\partial t} + \frac{\partial}{\partial s}(nV) = S, \tag{1}$$

$$\frac{\partial}{\partial t}(m_{\mathrm{i}}nV) + \frac{\partial}{\partial s}(m_{\mathrm{i}}nV^2 + nT_{\mathrm{i}} + nT_{\mathrm{e}} + \pi_{\mathrm{i}}^{\mathrm{eff}}) = M_{\mathrm{m}}, \tag{2}$$

author's e-mail: s12tk026@gmail.com

*) This article is based on the presentation at the 26th International Toki Conference (ITC26).

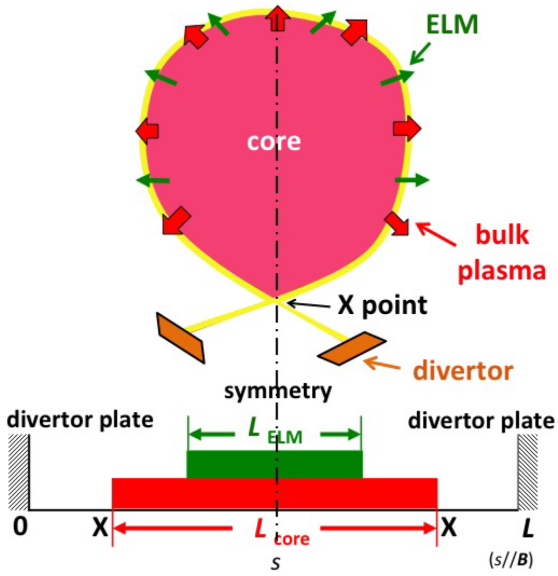

Fig. 1 Schematic system of 1D SOL-DIV plasma. Steady-state core source is given in the red region between X point to X point (parallel length $L_{\rm core}$), and the pulsed ELM source is given within a green region (parallel length $L_{\rm ELM}$).

$$\frac{\partial}{\partial t}\left(\frac{1}{2}m_{\rm i}nV^2+\frac{3}{2}nT_{\rm i}\right)+\frac{\partial}{\partial s}\left(\frac{1}{2}m_{\rm i}nV^3+\frac{5}{2}nT_{\rm i}V+q_{\rm i}^{\rm eff}\right) = Q_{\rm i}+\frac{3m_{\rm e}}{m_{\rm i}}\frac{n(T_{\rm e}-T_{\rm i})}{\tau_{\rm e}}-\frac{\partial}{\partial s}(\pi_{\rm i}^{\rm eff}V)-V\frac{\partial}{\partial s}(nT_{\rm e}), \quad (3)$$

$$\frac{\partial}{\partial t}\left(\frac{3}{2}nT_{\rm e}\right)+\frac{\partial}{\partial s}\left(\frac{5}{2}nT_{\rm e}V+q_{\rm e}^{\rm eff}\right) = Q_{\rm e}-\frac{3m_{\rm e}}{m_{\rm i}}\frac{n(T_{\rm e}-T_{\rm i})}{\tau_{\rm e}}+V\frac{\partial}{\partial s}(nT_{\rm e}). \quad (4)$$

Here, conductive heat fluxes and viscous flux are estimated by harmonic averages as below.

$$q_{\rm i/e}^{\rm eff}=\left(\frac{1}{q_{\rm i/e}^{\rm SH}}+\frac{1}{q_{\rm i/e}^{\rm FS}}\right)^{-1}, \quad \pi_{\rm i}^{\rm eff}=\left(\frac{1}{\pi_{\rm i}^{\rm BR}}+\frac{1}{\pi_{\rm i}^{\beta}}\right)^{-1}, \quad (5)$$

where $q_{\rm i/e}^{\rm SH}$ is Spitzer-Härm heat flux, $q_{\rm i/e}^{\rm FS}=\alpha_{\rm i/e}nT_{\rm i/e}v_{\rm t,i/e}$ is free-streaming heat flux with limiting factors of $\alpha_{\rm i}=0.5$, $\alpha_{\rm e}=0.2$ and $v_{\rm t,i/e}=(T_{\rm i/e}/{\rm m}_{\rm i/e})^{1/2}$ is the thermal velocity. The symbol $\pi_{\rm i}^{\rm BR}$ is Braginskii viscous flux, and $\pi_{\rm i}^{\beta}=\beta nT_{\rm i}$ is collisionless viscous flux with a limiting factor $\beta=0.7$. Transport of neutral particles is also described by a fluid model based on the first-flight corrected diffusion model [8].

$$\frac{\partial n_{\rm n,recy}^{\rm out}}{\partial t}+\frac{\partial}{\partial x}(n_{\rm n,recy}^{\rm out}V_{\rm n,recy}^{\rm out})=S_{\rm n,recy}^{\rm out}-n_{\rm n,recy}^{\rm out}\nu_{\rm L,recy}, \quad (6)$$

$$\frac{\partial n_{\rm n,recy}^{\rm inn}}{\partial t}+\frac{\partial}{\partial x}(n_{\rm n,recy}^{\rm inn}V_{\rm n,recy}^{\rm inn})=S_{\rm n,recy}^{\rm inn}-n_{\rm n,recy}^{\rm inn}\nu_{\rm L,recy}, \quad (7)$$

$$\frac{\partial n_{\rm n,diff}}{\partial t}+\frac{\partial}{\partial x}\left(-D_{\rm n}\frac{\partial n_{\rm n,diff}}{\partial x}\right)=S_{\rm n,diff}-n_{\rm n,diff}\nu_{\rm L,diff}, \quad (8)$$

Table 2 Basic calculation conditions.

Energy source	Particle source
$P_{\rm att}$ = 4 MW	$\Gamma_{\rm att}=2.0\times10^{22}$ /s
$P_{\rm det}$ = 2 MW	$\Gamma_{\rm det}=3.0\times10^{22}$ /s
$P_{\rm ELM}$ = 33 MW	$\Gamma_{\rm ELM}=1.0\times10^{23}$ /s

where the coordinate x is in the poloidal direction and $x=s\cdot\sin\theta$. Definitions of the variables in Eqs. (6 - 8) are described in Ref. [3]. We impose the boundary conditions at the sheath entrances as shown in Eqs. (9 - 11).

$$M\equiv\frac{V}{C_{\rm s}}=1, \quad (9)$$

$$\frac{1}{2}m_{\rm i}nV^3+\frac{5}{2}nT_{\rm i}V+q_{\rm i}^{\rm eff}=\gamma_{\rm i}nT_{\rm i}V, \quad (10)$$

$$\frac{5}{2}nT_{\rm e}V+q_{\rm e}^{\rm eff}=\gamma_{\rm e}nT_{\rm e}V, \quad (11)$$

where M is Mach number, $C_{\rm s}=((\gamma_{\rm A}T_{\rm i}+T_{\rm e})/m_{\rm i})^{1/2}$ is plasma sound speed and ion specific heat ratio $\gamma_{\rm A}=1$. Ion and electron heat fluxes at the sheath entrance are described by using the sheath heat transmission factors $\gamma_{\rm i}=4$ and $\gamma_{\rm e}=5$.

Table 2 shows the basic calculation conditions. First, we put energy and particle sources ($P_{\rm att}$, $\Gamma_{\rm att}$) for the steady-state attachment or ($P_{\rm det}$, $\Gamma_{\rm det}$) for the steady-state detachment in the core region. Then we introduce a pulsed type I ELM with energy and particle sources ($P_{\rm ELM}$, $\Gamma_{\rm ELM}$) from $t=t_0=0.3$ ms. The ELM crash duration $\Delta t_{\rm ELM}=200$ µs is unchanged in the present research.

3. Result

3.1 Type I ELM

The heat flux to the target plate after an ELM crash in the detachment starts to increase with a delay of ∼ 30 µs, contrary to the sudden increase in the attachment in Fig. 2 (a). It is also found in Fig. 2 (b) that the difference between electron heat flux and ion heat flux to the plate becomes much larger in the detachment, while their heat fluxes are similar in the attachment. The above delay is caused by the transition process from detachment to attachment.

Because of the strong equipartition between ion and electron temperatures in detachment, the ion heat is transferred to electrons before reaching the divertor plate as shown in Fig. 3, where the equipartition heat flux is the line integral from the source region to the target for equipartition power density $Q_{\rm eq}=3(m_{\rm e}/m_{\rm i})n(T_{\rm i}-T_{\rm e})/\tau_{\rm e}$. Therefore, the ion heat flux to the target is reduced.

3.1.1 Reverse flow in detachment

The reverse flow is observed near the target plate after an ELM incidence in the detachment. In the above calculations, we consider carbon impurity and its density fraction of $r_{\rm imp}=1.0$ %. Because $r_{\rm imp}$ is a key factor for the de-

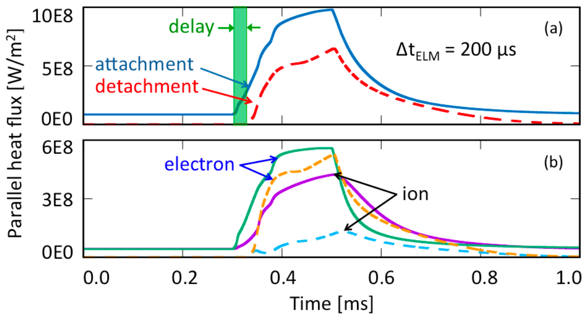

Fig. 2 (a) Comparison of time development of total parallel heat fluxes in attachment and detachment. (b) Ion and electron heat fluxes included in total heat fluxes. Solid and dashed lines represent attachment and detachment, respectively.

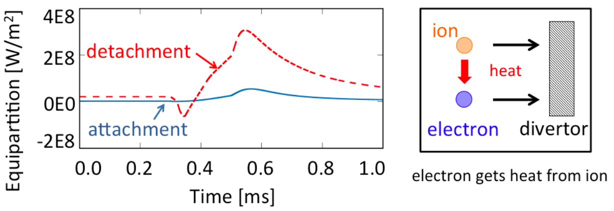

Fig. 3 Comparison of time developments of parallel heat flux of equipartition for attachment (solid line) and detachment (dashed line). Ion heat is transferred to electrons before reaching the divertor plate (right schematic).

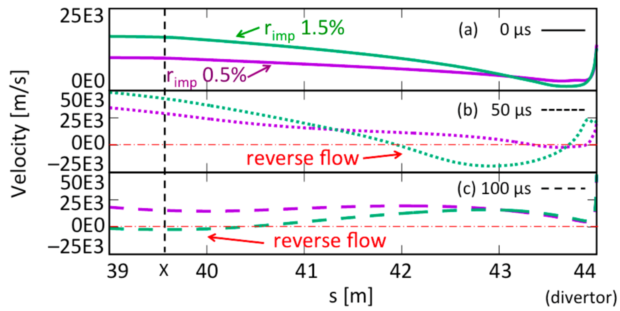

Fig. 4 Spatial distribution of flow velocity at (a) 0 μs after an ELM occurs in detachment, (b) 50 μs and (c) 100 μs. Purple and green lines represent cases of r_{imp} = 0.5 % and 1.5 %, respectively.

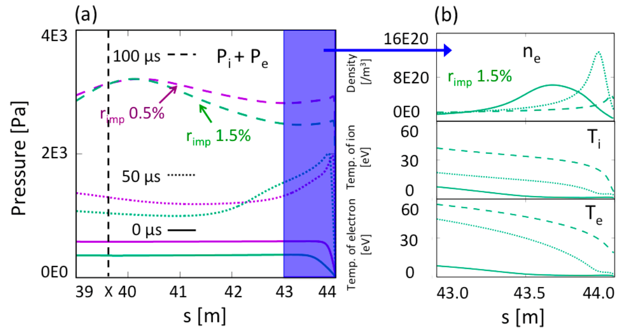

Fig. 5 Temporal change of spatial distributions after an ELM in detachment (solid, dotted and dashed lines represent the line $t - t_0$ = 0 μs, 50 μs, and 100 μs, respectively): (a) plasma pressure, $P_i + P_e$, for the range s = 39 - 44 m. (b) density n_e, ion temperature T_i, and electron temperature T_e near the target s = 43 - 44 m for the case of r_{imp} = 1.5 %.

tachment, we vary r_{imp} from 0.5 % to 1.5 % to investigate the characteristics of reverse flow. As shown in Fig. 4 (a) at $t - t_0 = 0$ μs, the flow velocity in front of the target (s = 43 - 44 m) becomes smaller when we raise r_{imp}. As time passes after ELM, the magnitude of reverse flow for higher r_{imp} becomes larger and the peak of reverse flow leaves farther away from the target, even reaches to an upper stream above x point as seen in Figs. 4 (b) at $t - t_0 = 50$ μs and (c) at $t - t_0 = 100$ μs.

For the details, we investigate the spatial distribution of plasma pressure $P_i + P_e$, density n_e and ion temperature T_i and electron temperature T_e as shown in Fig. 5. Here, we consider that the ion and electron temperatures rise quickly due to ELM, the plasma pressure in front of the target becomes extremely high, and then the plasma flow is reversed to the upstream.

3.2 Grassy ELMs

We investigate grassy ELMs with smaller amplitude. Parameters of ELM are P_{grassy} = 3.3 MW ~ 0.1 $P_{\mathrm{type\,I\,ELM}}$, Γ_{grassy} = 1.48 × 10^{22}/s ~ 0.15 $\Gamma_{\mathrm{type\,I\,ELM}}$, and Δt_{ELM} = 200 μs. At first, we put two ELM pulses with 13 ms interval, and confirm that the repetition of the heat flux form at the target is realized in this model as shown in Fig. 6. Next, we put five ELM pulses with frequency f_{grassy} = 2000 Hz into attachment and detachment as shown in Fig. 7. We find that the difference of ELM heat fluxes between attachment and detachment in grassy ELM case is much larger than that in type I ELM case. It implies that detached plasma is effective in lower power of ELM. On the other hand, we find a compound phenomenon of the accumulation of heat flux between the first ELM pulse and the second pulse in detachment. The second peak of the heat flux becomes higher than the first one.

These dynamic responses are strongly dominated by the radiation effect. Figure 8 shows the difference in radiation heat flux between for detachment and for attachment, where the radiation heat flux is the line integral from the source region to the target for radiation power density $Q_{e,rad}$. Radiation power in detachment is higher by two order than that in attachment all the time.

3.2.1 Radiation effect in detachment

In the above simulations, we adopt a simple radiative cooling model (Model I), $Q_{e,rad} = L_z(T_e) n_z n_e$, and assume that the profile of impurity density is unchanged by the ELM pulse; $n_z(s) = n_z(s, t = t_0) = r_{imp} n_e(s, t = t_0)$ at r_{imp} = 1 %. Radiation efficiency $L_z(T_e)$ of the carbon is calculated by taking into account of impurity recycling ef-

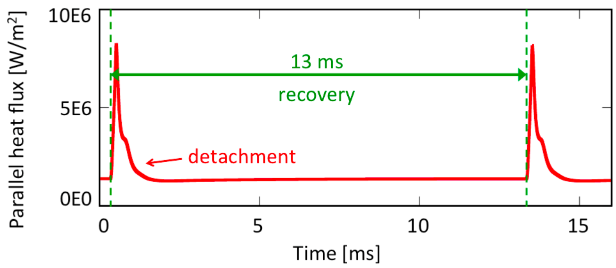

Fig. 6 Repetition of parallel heat flux in detachment for two grassy ELM pulses with 13 ms interval.

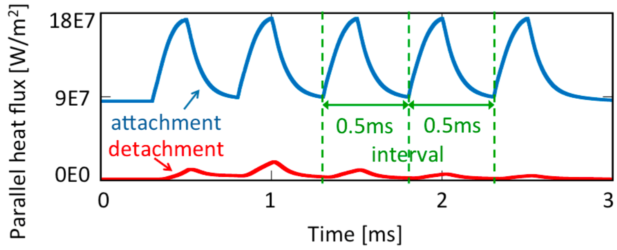

Fig. 7 Time development of parallel heat flux in attachment (blue line) and detachment (red line) for five grassy ELM pulses with f_{grassy} = 2000 Hz.

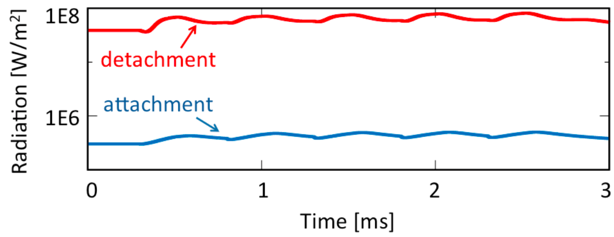

Fig. 8 Time development of parallel heat flux of radiation in attachment (blue line) and detachment (red line).

fect ($n_e\, \tau_{recycle} \sim 10^{15}\ \mathrm{s \cdot m^{-3}}$).

Now we examine the sensitivity on the radiation model. We introduce another simple radiative cooling model (Model II), $Q_{e,rad} = L_z(T_e) r_{imp} n_e^2$, where we assume that the impurity fraction r_{imp} = 1 % is kept constant and the impurity density is varied much by the ELM pulse; $n_z(s,\ t) = r_{imp} n_e(s,\ t)$. We find in attachment case as shown by Fig. 9 (a) that the amounts of ELM heat fluxes for Model II become smaller than that for Model I. On the other hand in detachment case as shown by Fig. 9 (b), first and second ELM-pulse heat fluxes for Model II are larger than those for Model I. After the third ELM-pulse, the heat flux for Model II decreases more rapidly than that for Model I. Figure 10 shows the radiation flux in detachment. The radiation flux for Model II is smaller than that for Model I at the beginning, but becomes larger than that for Model I in the end.

In addition to the impurity density response, the ELM pulse can affect the impurity recycling and resultantly af-

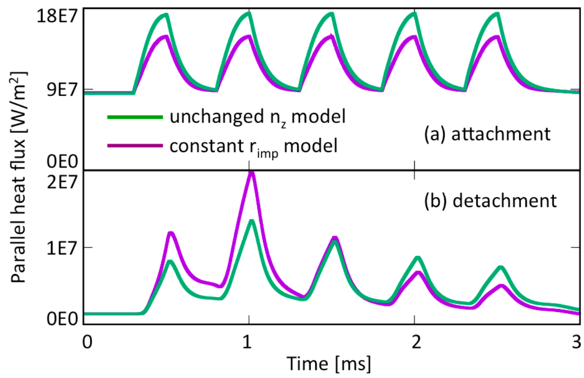

Fig. 9 Time development of parallel heat flux in (a) attachment and (b) detachment. Green and purple lines represent the cases of Model I (unchanged n_z) and Model II (constant r_{imp}), respectively.

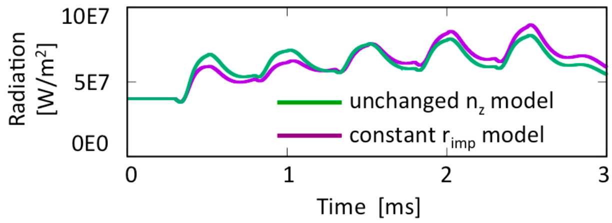

Fig. 10 Time development of radiation flux in detachment. Green and purple lines represent the cases of Model I and Model II, respectively.

fect $L_z(T_e)$. Improvement in the radiation model for the precise analysis is a future work.

4. Conclusion

We investigate the dynamic response of plasma detachment against the ELM using a one-dimensional fluid code. It is found that electrons get more heat from ions before reaching the divertor plate due to the strong equipartition in detachment. In addition, it is found that the reverse flow in the detachment is caused by ELM unbalancing the plasma pressure. The magnitude of reverse flow becomes larger and the peak of reverse flow leaves farther away from the target with the higher impurity fraction. Finally, we investigate the grassy ELMs in the detachment. It is found that the heat flux flowing to the target in the detachment is much smaller than that in the attachment due to the high radiation in the detachment. We find the accumulation of the heat flux between the first ELM pulse and the second one. Mechanism of the accumulation will be studied in the future. Since the radiation plays an important role for the dynamic response of detached plasma against ELM pulses, we study the sensitivity to the radiation model. Improvement of the model such as including the effect of finite plasma currents are future works.

[1] A. Loarte *et al.*, Nucl. Fusion **47**, S203 (2007).
[2] N. Ohno, J. Plasma Fusion Res. **92**, 877 (2016).
[3] S. Togo *et al*., Contrib. Plasma Phys. **56**, 729 (2016).
[4] H. Urano *et al*., Plasma Phys. Control. Fusion **45**, 1571 (2003).
[5] B.N. Rogers *et al*., Phys. Rev. Lett. **81**, 4396 (1998).
[6] M. Sugihara *et al*., Plasma Phys. Control. Fusion **45**, L55 (2003).
[7] S.I. Braginskii *Reviews of Plasma Physics* vol.1, p.205 (Consultants Bureau, New York, 1965).
[8] A.K. Prinja *et al*., J. Nucl. Mater. **196**-**198**, 340 (1992).